Published in final edited form as:
IEEE Trans Biomed Eng. 2010 January ; 57(1): 145–154. doi:10.1109/TBME.2009.2034533.

Microbubble-Size Dependence of Focused Ultrasound-Induced Blood–Brain Barrier Opening in Mice *In Vivo*

James J. Choi [Student Member, IEEE], **Jameel A. Feshitan**, **Babak Baseri**, **Shougang Wang [Member, IEEE]**, **Yao-Sheng Tung**, **Mark A. Borden [Member, IEEE]**, and **Elisa E. Konofagou*** **[Member, IEEE]**

J. J. Choi and Y.-S. Tung are with the Department of Biomedical Engineering, Columbia University, New York, NY 10027 USA (jamesjc@gmail.com)

J. A. Feshitan and M. A. Borden are with the Department of Chemical Engineering, Columbia University, New York, NY 10027 USA

B. Baseri was with the Department of Biomedical Engineering, Columbia University, New York, NY 10027 USA. He is now with St. George's University, St. George 11473, Grenada

S. Wang was with the Department of Biomedical Engineering, Columbia University, New York, NY 10027 USA. He is now with the National Semiconductor Corporation, Santa Clara, CA 95051-0695 USA

E. E. Konofagou is with the Department of Biomedical Engineering and Department of Radiology, Columbia University, New York, NY 10027 USA

Abstract

The therapeutic efficacy of neurological agents is severely limited, because large compounds do not cross the blood–brain barrier (BBB). Focused ultrasound (FUS) sonication in the presence of microbubbles has been shown to temporarily open the BBB, allowing systemically administered agents into the brain. Until now, polydispersed microbubbles (1–10 μm in diameter) were used, and, therefore, the bubble sizes better suited for inducing the opening remain unknown. Here, the FUS-induced BBB opening dependence on microbubble size is investigated. Bubbles at 1–2 and 4–5 μm in diameter were separately size-isolated using differential centrifugation before being systemically administered in mice (n = 28). The BBB opening pressure threshold was identified by varying the peak-rarefactional pressure amplitude. BBB opening was determined by fluorescence enhancement due to systemically administered, fluorescent-tagged, 3-kDa dextran. The identified threshold fell between 0.30 and 0.46 MPa in the case of 1–2 μm bubbles and between 0.15 and 0.30 MPa in the 4–5 μm case. At every pressure studied, the fluorescence was greater with the 4–5 μm than with the 1–2 μm bubbles. At 0.61 MPa, in the 1–2 μm bubble case, the fluorescence amount and area were greater in the thalamus than in the hippocampus. In conclusion, it was determined that the FUS-induced BBB opening was dependent on both the size distribution in the injected microbubble volume and the brain region targeted.

Keywords

Blood; brain barrier; brain drug delivery; focused ultrasound (FUS); microbubbles; opening; permeability

*(ek2191@columbia.edu)..

I. Introduction

THE EXCHANGE of molecules across the cerebral microvasculature is regulated by a unique interface known as the blood-brain barrier (BBB). Its major functions are to prevent toxins from entering the parenchyma and to maintain molecular environments necessary for proper neuronal firing [1], [2]. Through a combination of passive, transport, and metabolic barriers, nearly all systemically administered compounds larger than 400 Da are excluded from the brain's extracellular space, rendering thus many neurologically potent compounds ineffective [3]. As a result, potential therapeutic agents, such as inhibitors to enzymes (~1 kDa) and antibodies (30–300 kDa), will not reach their intended targets if administered systemically. The treatment of central nervous system (CNS) disorders will remain severely impaired until a method to deliver such large agents in the brain at a sufficient dose is shown to be effective [3].

Several brain drug delivery methods are being developed to overcome the BBB obstacle and include intracranial injections, mixing, or attaching agents with BBB-modifying chemicals (i.e., mannitol), and the chemical modification of agents to be delivered through endogenous transport systems [3]. However, the methods are either invasive or limited in spatial specificity. In this paper, we investigated focused ultrasound (FUS) applied after the systemic administration of ultrasound contrast agents (UCA) as the BBB opening method [4]. To our knowledge, this is the only known technique, out of those clinically used or under development, which concurrently delivers agents to the brain through the intact skull, locally (to a targeted volume), and transiently with the BBB closing within hours of its opening [3]–[5]. To this date, safety assessment has been comprised of histological analysis to determine the presence of apoptosis, neuronal death, and erythrocyte extravasations [6]–[9], and MRI to determine the presence of hemorrhage, macroscopic structural changes, and the timeline of BBB closure [4], [5], [10]. Comprehensive histological analyses of the damage within a few days of sonication revealed that, at specific acoustic parameters (i.e., pressure, frequency, pulse length, pulse repetition frequency, and duration), BBB opening can occur without widespread hemorrhage or neuronal damage [11], [12]. In light of the serious lack of effective clinical treatments of most CNS disorders, the safety profile of FUS-induced BBB opening reported to this date is promising for human applications.

In terms of efficacy, FUS-induced BBB opening has been shown to increase the BBB permeability to therapeutically relevant-sized agents, such as Omniscan (573 Da), Magnevist (938 Da) [4], [5], [10], Evans Blue [13], Trypan Blue [14], Herceptin (148 kDa) [13], doxorubicin (544 Da) [15], and rabbit anti-Aβ antibodies [14]. However, the magnitude of this permeability increase, the spatial distribution of the delivered agents within the targeted volume, and the dependence of both on the agent's molecular weight have not been extensively investigated in these studies. In order to study these characteristics, dextrans at three distinct molecular weights (3, 70, and 2000 kDa) were employed as model agents [16], [17]. It was found that, although compounds larger than 400 Da can be delivered, there is a size exclusion threshold that remains. The 3-kDa dextran was more evenly distributed and at a higher concentration than that of the 70-kDa dextran. Dextrans were also deposited at larger amounts proximal to larger vessel branches such as the internal and external transverse hippocampal vessels, and the vessels within the thalamus, when compared with other regions in the targeted hippocampus. As a result, although large agents have been shown to be delivered through the BBB, there remain concerns regarding the effective concentration and spatial distribution of trans-BBB delivered compounds.

To date, all FUS-induced BBB opening studies utilized UCAs (i.e., Definity, SonoVue, and Optison) with either a protein or lipid shell and a stabilized gas core. The original development of these UCAs was to provide image contrast while remaining safe for

systemic administration by restricting the bubble size to below 10 μm. FUS-induced BBB opening, in a stark difference, requires that the preformed microbubbles be present to allow for an increase of the BBB's permeability in order to modulate the biological environment, albeit temporarily. At the low acoustic pressures typically used in FUS-induced BBB opening (<1 MPa peak-rarefactional), microbubbles are a key component since opening does not occur without their presence in the vasculature [4], [5], [10]. Thus, in this paper, we hypothesize that microbubbles can be specifically designed for the purpose of inducing BBB opening and predicting its characteristics. To do this, we noted several studies by our group and others on acoustic cavitation, the cerebral vasculature, and their influence on BBB opening. First, the BBB opening acoustic pressure threshold has been previously shown to be below the inertial cavitation threshold [11], thus indicating that noninertial cavitation may be one of the causes for opening. Second, the BBB exists along cerebral capillaries, which are 4–8 μm in diameter [18], therefore, bubbles smaller than 8 μm were used. The vessel size also describes the constrained environment, within which these bubbles are interacting. Several simulations and *in vitro* studies of microvessels have shown that the bubble's resonance frequency, its expansion ratio, its pressure threshold for inertial cavitation and fragmentation, its translational velocity, and lifetime of stable oscillation are all dependent on the bubble size and vessel diameter [19]–[26]. Third, we observed that, when sonicating in the presence of polydispersed SonoVue, not only were agents delivered trans-BBB but they were also concentrated at or near large vessels [27]. Thus, we hypothesized that a particular bubble size, within the larger size distribution range, causes the specific desirable effect of BBB opening, i.e., safe and localized.

The purpose of this paper is to determine the BBB opening dependence on microbubble size distribution. Microbubbles were size-isolated into 1–2 and 4–5 μm diameter ranges with differential centrifugation [28], deemed small enough to perfuse the cerebral vasculature while sufficiently large to induce the required mechanical stress on the vessel wall. For each bubble set, the BBB opening acoustic pressure threshold was identified and the safety was evaluated using histological analysis. In addition, the extent of BBB opening in different brain regions, which have different capillary densities [29], [30], was compared. Finally, the size distribution of systemically administered microbubbles and the vasculature they circulate in were shown to be key factors in the FUS-induced BBB opening.

II. Materials And Methods

A. Ultrasound Equipment

A single-element, spherical-segment FUS transducer (center frequency: 1.525 MHz, focal depth: 90 mm, radius: 30 mm; Riverside Research Institute, New York, NY, USA) was driven by a function generator (Agilent, Palo Alto, CA, USA) through a 50-dB power amplifier (E&I, Rochester, NY, USA) to generate therapeutic acoustic waves. A pulse-echo transducer (center frequency: 7.5 MHz; focal length: 60 mm), which was used as an imaging transducer, was positioned through a central, circular opening of the FUS transducer so that their foci were aligned. The imaging transducer was driven by a pulser–receiver system (Olympus, Waltham, MA, USA) connected to a digitizer (Gage Applied Technologies, Inc., Lachine, QC, Canada). A cone-shaped chamber filled with degassed and distilled water was mounted on the transducer system and capped with an acoustically transparent latex membrane (Trojan; Church & Dwight Co., Inc., Princeton, NJ, USA) in order to contain the water (see Fig. 1). The transducers were attached to a computer-controlled 3-D positioning system (Velmex Inc., Lachine, QC, Canada).

The details of the FUS transducer's acoustic pressure amplitude and beam profile measurements have been previously described [5], [10]. In brief, the pressures reported in this study were calculated by measuring the peak-rarefactional pressure amplitudes with a

needle hydrophone (needle diameter: 0.2 mm; Precision Acoustics Ltd., Dorchester, Dorset, U.K.) in degassed water while accounting for 18.1% attenuation through the parietal bone of the mouse skull. The lateral and axial full-width at half-maximum (FWHM) intensity was measured to be approximately 1.32 and 13.0 mm, respectively.

B. Size Isolated Microbubbles

Microbubbles comprised of a 1,2-distearoyl-*sn*-glycero-3-phosphocholine (DSPC) and polyoxyethylene-40 stearate (PEG40S) lipid-shell with a perfluorobutane (PFB) gas core were manufactured in-house. Size-selected microbubbles were isolated from a polydispersed microbubble distribution using a method developed by Feshitan *et al.* (2008). In brief, acoustic emulsification was first used to generate a polydispersed microbubble distribution [28]. Using Stokes' equation [31], which calculates the rise velocity of a buoyant particle relative to the bulk fluid under creeping flow conditions, bubble suspensions were centrifuged at a specific relative centrifugal force and duration. The resulting cake (portion of the centrifuged tube located radially inward) or infranatant (portion of the centrifuged tube located radially outward) was resuspended to preserve either larger or smaller bubbles, respectively. The centrifugation and resuspension process was repeated several times until the desired 1–2 or 4–5 μm diameter range was obtained. The final solution was redispersed to 1-mL of 20 volume percent glycerol solution in PBS and stored in a 2-mL serum vial with PFB headspace.

The final microbubble size distribution in each vial was determined by laser light obscuration and scattering (Accusizer 780A, NICOMP Particle Sizing Systems, Santa Barbara, CA, USA) before and after its use in the FUS-induced BBB opening experiments. In all BBB opening experiments and for both sets of bubbles, the total concentration was kept constant at approximately 8.5×10^8 number of bubbles per mL. In order to ensure accuracy of concentration, the bubbles were generated at an initial yield larger than the desired concentration and then diluted in PBS 1 min before intravenous injection into the mouse.

C. Preparation of Animals

All procedures involving animals were approved by the Columbia University Institutional Animal Care and Use Committee. A total of 28 wild-type mice (strain: C57BL/6, mass: 28.0 ± 4.5 g, sex: male; Harlan, Indianapolis, IN, USA) were used in this study. The mice were anesthetized using 1.25–2.50% isoflurane (SurgiVet, Smiths Medical PM, Inc., Wisconsin, USA) throughout both the BBB opening and transcardial perfusion procedures.

D. Blood–Brain Barrier Opening Protocol

Each mouse was anesthetized and placed prone with its head immobilized by a stereotaxic apparatus (David Kopf Instruments, Tujunga, CA, USA) (see Fig. 1). The mouse hair was removed using an electric trimmer and a depilatory cream. A degassed water-filled container sealed at the bottom with thin, acoustically and optically transparent, Saran Wrap (SC Johnson, Racine, WI, USA) was placed on top of the mouse head while ultrasound coupling gel was used to eliminate any remaining impedance mismatch between the two surfaces. The transducers were then submerged in the water of the container with its beam axis perpendicular to the surface of the skull.

A grid positioning method to target the mouse brain was then used as previously described [10]. In brief, a metallic grid was placed in alignment with the mouse skull's sutures, which were visible through the intact skin. The grid was then imaged using the pulse-echo transducer in a raster-scan, and, since the foci of the two transducers were aligned, the position of the FUS transducer relative to the sutures was known. The FUS transducer was

moved 2.25 mm laterally of the sagittal suture and 2.0 mm anterior of the lambdoid suture [see Fig. 2(a)]. This corresponded to the focus overlapping with the left hippocampus and the lateral portion of the thalamus [see Fig. 2(b)]. This target was selected, because the parietal bone allowed for the lowest attenuation and beam distortion to the 1.525 MHz ultrasound frequency used. More importantly, the hippocampus is an anatomical region that is easy to identify and trace, is a comprehensively studied brain region, and is a potential therapeutic target (i.e., early onset of Alzheimer's disease is typically detected at the hippocampus). The right hemisphere was not targeted and was used as a control. The grid positioning method was sufficiently precise to have the FUS beam consistently overlap with the hippocampus of the brain. No craniotomy was performed.

A 25-μL bolus of either 1–2 or 4–5 μm diameter bubbles was injected into the tail vein one minute prior to sonication. For the 1–2 bubble set, pulsed FUS (pulse rate: 10 Hz, pulse length: 20 ms, duty cycle: 20%) was applied at 0.30 (n = 4), 0.46 (n = 3), or 0.61 (n = 4) MPa peak-rarefactional pressure in a series of two 30-s intervals of sonication at a single location. A 30-s interval between the two allowed for residual heat to dissipate and microbubbles to reperfuse the cerebral vasculature undisturbed by the acoustic wave [5]. The same experiment was repeated for the 4–5 μm bubble set, but acoustic peak-rarefactional pressures were set at 0.15 (n = 4), 0.30 (n = 5), or 0.46 (n = 3) MPa. The pressure ranges used were based on our previous studies with Definity [16]. Since our previous work has shown that the vascular characteristics (i.e., vascular density) in the sonicated region may influence the extent of BBB opening, the sonication procedure was performed once and at a single location in each mouse brain in order to more accurately compare BBB opening pressure thresholds.

Approximately 10 min after FUS-induced BBB opening, 3-kDa Texas Red-tagged dextran, which was measured by dynamic light scattering to be 2.33 ± 0.38 nm in diameter [16], was injected into the femoral vein. After a 20-min interval, which enabled the dextran to circulate throughout the vasculature, the mice were transcardially perfused with 30 mL of phosphate buffer saline (138 mM sodium chloride, 10 mM phosphate, pH 7.4) and 60 mL of 4% paraformaldehyde. The brain was extracted from the skull, postfixed in paraformaldehyde overnight, and then prepared for either frozen (n = 22) or paraffin sections (n = 6). The frozen sectioning protocol provided an efficient means of analyzing fluorescence in order to determine the BBB opening threshold. Meanwhile, the paraffin sections allowed for analysis of both the delivery of dextran and safety at the pressure thresholds, i.e., 0.46 and 0.30 MPa with the 1–2 and 4–5 μm bubbles, respectively.

In preparation of frozen sectioning, the brain was cryoprotected by soaking it in 30% sucrose overnight. The brain was then embedded in optimum cutting temperature compound (Sakura Tissue-Tek O.C.T. Compound; Torrance, CA, USA), frozen in a square mold, and sectioned using a cryostat into 200-μm slices in the horizontal orientation. In preparation for paraffin sectioning, the brain was embedded in paraffin. From the dorsal side of the brain, 1.2 mm was trimmed away and then 12 levels were obtained with 80-μm bypassed between levels. At each level, six sections at 6-μm were obtained, two were stained with hematoxylin and eosin (H&E), and four remained unstained for fluorescence imaging to detect the trans-BBB delivered dextran.

E. Histological Image Analysis

Bright field and fluorescent images of the frozen sections were acquired using an inverted light and fluorescence microscope (IX-81; Olympus, Melville, NY, USA) with a motorized stage-scanner. Paraffin sections were imaged using an upright light and fluorescence microscope (BX61; Olympus, Melville, NY, USA). In both cases, the Texas Red-tagged dextran was excited at 568 ± 24 nm while emissions were filtered for 610 ± 40 nm.

In the case of frozen sections, horizontal sections were chosen at defined cross sections as depicted in Figs. 4 and 5. A 3 × 3 mm^2 region of interest (ROI) in the bright field images was selected (see Figs. 4 and 5) using Adobe Photoshop (San Jose, CA, USA) and the hippocampus and thalamus were manually outlined. The outlines were then loaded into MATLAB (Natick, MA, USA) and used to isolate the hippocampus on the fluorescence images. MATLAB routines were used to calculate the spatial average and standard deviation of fluorescence in the control and targeted ROIs. Based on these values, the relative increase in fluorescence was then calculated by subtracting the spatially averaged fluorescence in the right ROI from the spatially averaged fluorescence in the left ROI and then dividing the calculated value by the spatially averaged fluorescence in the right ROI.

F. Statistical Analysis

Differences between two sets of values were determined using a statistical analysis. Following the calculation of the mean and standard deviation in the change of fluorescence of the left over the right hippocampus, a Student's *t*-test was performed. The same comparison amongst the different sets of values for the increase in area of fluorescence was made. In all comparisons, a difference in fluorescence at $P < 0.05$ was considered statistically significant.

III. Results

A. Microbubble Stability

A typical size distribution for the 1–2 and 4–5 μm diameter bubbles is depicted in Fig. 3 as number-weighted [see Fig. 3(a)] and volume-weighted [see Fig. 3(b)] percentage of the total number of bubbles and gas volume, respectively. In both instances, there was minimal size overlap between the two bubble sets. In order to test for stability, size distribution measurements were acquired from the same vial before and between 6 and 11 h after the BBB opening experiments.

For both sets of bubbles, the number-weighted and volume-weighted mean and median bubble sizes, and the polydispersity index (PI), were quantified (see Table I). The PI, which was defined in Feshitan *et al*. (2008) as the volume-weighted mean diameter divided by the number-weighted mean diameter, was calculated to assess size uniformity. The 1–2 μm bubbles had number-weighted and volume-weighted mean and median diameters within the 1–2 μm range and a good PI value of 1.2 ± 0.1 before the BBB opening experiments (see Table I). After the experiment, the PI increased to 2.0 ± 0.9, as indicated by the increased discrepancy between number-weighted and volume-weighted mean diameters. However, this distribution remained distinct to the 4–5 μm bubbles. The 4–5 μm bubbles had volume-weighted mean and median values within the 4–5-μm range and a good PI value of 1.5 ± 0.1. The number-weighted diameters were below the 4-μm target lower limit, but were still deemed distinct from the 1–2 μm bubble set. Meanwhile, the volume-weighted diameter mean and median were 5.0 ± 0.2 and 4.3 ± 0.1 μm, respectively. The bubble size distribution did not significantly change after the BBB opening experiments as indicated by the PI value of 1.4 ± 0.1.

B. Ultrasound-Induced Blood–Brain Barrier Opening

Following systemic injection of 1–2 μm bubbles, the sonication induced an increase in fluorescence intensity at 0.46 and 0.61 MPa [see Fig. 4(a) and (c)] while no increase was observed at 0.30 MPa. At 0.46 MPa, increased fluorescence was observed, but they were not consistent across enough mice to unequivocally indicate BBB opening ($P > 0.1$). Regardless, a statistically significant increase was observed at 0.61 MPa. Following the systemic administration of 4–5 μm bubbles, sonication induced a fluorescence increase at 0.30, 0.46,

and 0.61 MPa [see Fig. 5(a), (c), and (e)] that was statistically significant ($P < 0.05$) while no fluorescence increase was observed at 0.15 MPa (see Fig. 6). At above 0.30 MPa, fluorescence was observed not only at the fissures and along large vessels, but also diffusely throughout the hippocampus and thalamus.

For each ROI and acoustic pressure, 4–5 μm bubbles produced greater increases in fluorescence compared with the 1–2 μm bubbles. In addition, the pressure amplitude threshold where significant fluorescence was observed was lower for the 4–5 μm bubbles than for the 1–2 μm bubbles. This implied that a lower acoustic pressure was required to induce BBB opening for the larger (4–5 μm) bubbles. It was qualitatively noted that there were regional variations in fluorescence within the sonicated region [see Fig. 4(a) and (c)]. Therefore, we compared enhancement in fluorescence in the thalamus and hippocampus at 0.61 MPa in the 1–2 μm bubble case. A clear difference in fluorescence increase was detected ($P < 0.01$).

C. Safety

Mouse brains were assessed for histological damage as defined by the presence of discrete damage sites, such as neuronal damage (dark neurons), gross hemorrhage, vacuolization, and small erythrocyte extravasations [32]. Three of the six mice were sonicated at 0.46 MPa in the presence of 1–2 μm bubbles while the other three were sonicated at 0.30 MPa in the presence of 4–5 μm bubbles. Sonication in the presence of 1–2 μm bubbles clearly depicts BBB opening at 0.46 MPa [see Fig. 8(a) and (b)]. The 6-μm thick sections immediately neighboring the sections depicted in Fig. 8(a) and (b) were H&E-stained [see Fig. 8(c)–(f)]. No discrete damage sites were detected in the 12 sections analyzed. In some sections, single erythrocytes were qualitatively observed, but they also appeared in the control, contralateral hemisphere, thus indicating that this might be due to histological artifacts. In addition to this, it was difficult to determine whether these erythrocytes remained within vessels or whether they had extravasated. Sonication at 0.30 MPa in the presence of 4–5 μm bubbles also resulted in BBB opening [see Fig. 9(a) and (b)] and no discrete damage sites were observed [see Fig. 9(c) and (d)]. Small erythrocyte extravasations were observed in both the sonicated and control hemispheres [see Fig. 9(e) and (f)]. For all pressures and bubbles tested, regions, where a high intensity of fluorescence was observed, were not associated with any dead neurons, necrotic sites, or hemorrhage [see Figs. 8(e) and (f) and 9(e) and (f)].

IV. Discussion

Microbubbles were carefully designed to evaluate their influence on BBB opening. The 1,2-distearoyl-*sn*-glycero-3-phosphocholine (DSPC) and polyoxyethylene-40 stearate (PEG40S)-shelled microbubble with a PFB gas core was shown to induce BBB opening; thus, adding to the group of pre-formed microbubbles capable of opening the BBB (i.e., in addition to Definity, SonoVue, and Optison). Several methods for generating monodisperse microbubbles exist and include flow focusing [33], [34], T-junctions [35] and electrohydrodynamic atomization [36]. However, differential centrifugation was unique in that it allowed for the large volume of size-isolated bubbles required for our study. The bubbles generated from this method were also previously characterized to be stable over a period of at least two days, which was sufficient for the purpose of this study [28]. Compared with the previously reported study [28], we experienced a greater change in the PI in less than a day, but this may be due to the repeated extraction of large bubble volumes from the vial with little volume remaining for proper size distribution measurement with the Accusizer. After taking this potential artifact into account, we believe that the bubble's mean and median diameters did not change from before to after the BBB opening experiments as much as Table I may suggest. Even in the case where Table I indicated the actual maximum

change in bubble diameter, the isolated size peaks remained distinct. Another important aspect of the experimental design was that the bubble concentration, as opposed to the volume fraction, was kept constant across the different size distributions tested. This decision was made, because of an assumption: BBB opening occurs discretely, i.e., the sites of molecular leakage are highly correlated with the instantaneous locations of the bubbles at the time of sonication. In the case, where the bubble concentration or volume fraction was kept constant, it was deemed that our method of analysis was sensitive enough to detect minute increases in fluorescence and, therefore, the BBB opening acoustic pressure threshold in each bubble case. The overall concentration may have no effect on whether BBB opening occurs, but it may have an effect on the number of BBB opening sites along each capillary, and thus the amount of fluorescent-tagged dextran infusing the parenchyma.

The lowest peak-rarefactional pressure that induced BBB opening was 0.46 MPa for the 1–2 μm bubbles and 0.30 MPa for the 4–5 μm bubbles (see Fig. 6). Here, we defined the threshold as the lowest acoustic pressure necessary for inducing BBB opening. Statistically significant BBB opening with the 1–2 μm bubbles was observed only at 0.61 MPa, but since BBB opening was observed at 0.46 MPa for at least one mouse, and in all the brain sections for that mouse, indicated that BBB opening could be produced at the lower pressure amplitude. According to this definition, the acoustic pressure threshold for BBB opening fell between 0.30 and 0.46 MPa for the 1–2-μm bubbles and between 0.15 and 0.30 MPa for the 4–5-μm bubbles. The reason for this difference in the threshold is not clear. Recent studies have shown that with a decreasing vessel diameter, there is decrease in the expansion ratio [19], [22] and increase in the pressure threshold for inertial cavitation or fragmentation [24]. This may be due to the bubble's change in resonance frequency or its constraint within a microvessel [23], [25]. This, and our previous study, showed that two types of increased fluorescence were observed: spatially distributed regions of fluorescence due to the delivery of agents across the BBB and concentrated regions of fluorescence near or along large vessel walls [17].

The first, more diffuse, observed fluorescence may be due to the type of bubble behavior in capillaries. A small bubble (1–2 μm) is not as constrained as a larger bubble (4–5 μm) during flow through a capillary (4–8 μm) [18]. If mechanical stress to the vessel wall due to the acoustically driven bubble size expansion were the primary cause for BBB opening, then a higher acoustic pressure amplitude would be necessary to induce this effect for the 1–2-μm than for the 4–5-μm bubbles. Given their comparable size to the capillary diameter, the 4–5-μm bubbles may have higher inertial cavitation and fragmentation thresholds than if they were in a larger vessel [22]. Therefore, applying low (0.30 MPa) acoustic pressure to the 4–5 μm bubble may have been sufficient to initiate stable bubble oscillations that induced repeated stress against the wall, thereby opening the BBB more efficiently. This same pressure may not have been sufficient to cause the 1–2 μm bubbles to have the same desired therapeutic effect.

The second, more concentrated, observed fluorescence may be explained by the larger vessels that the bubbles are interacting with. One possible rationale behind this observation is that in larger vessels (i.e., venules, arterioles, veins, and arteries), the threshold of inertial cavitation and fragmentation decreases when compared with smaller vessels (i.e., capillaries) [24]. If free bubbles were sonicated at the frequency used in our study, then 1–2 μm bubbles would be more likely to undergo inertial cavitation or fragmentation than 4–5-μm bubbles [37]. Figs. 4 and 5 qualitatively indicate that we may have higher fluorescence concentrated near the vasculature in the 1–2-μm than in the 4–5-μm bubble case. Another possible rationale is related to bubble reperfusion and the pulse repetition frequency. Previous studies have shown that, if the pulse results in microbubble fragmentation and if the pulse repetition frequency is too high, then the microbubbles will be destroyed before

they perfuse the microvasculature, thereby decreasing the therapeutic efficacy [38], [39]. In this paper, bubble destruction in the larger vessels may be associated with concentrated fluorescence at or near them (see Figs. 4 and 5), which may have prevented them from completely perfusing the hippocampal and thalamic microvasculature. The aforementioned explanations of the two different types of fluorescence observed are, however, speculative and further studies will be carried out to determine the underlying causes. However, from the findings presented, it can be concluded that matching the bubble size to the acoustic parameters used and targeted vasculature might help to control the size and degree of the desired therapeutic effect.

The mouse was selected as the animal to use, because several transgenic models of neurodegenerative diseases have been recently established for it [40], and it is the most comprehensively studied animal in neuroscience. In addition, and more relevant to this paper, its vascular anatomy and density are well understood [41]–[43]. Because of the aforementioned factors and the need for a large sample size in a parametric study, an accurate and high throughput FUS targeting system specific for the mouse brain was previously developed by our group and used in this paper [10]. The accuracy of the system permitted not only good reproducibility across different mice, but also allowed for the comparison of BBB opening effects in different regions within the sonicated volume. Our previous work [27], as well as Figs. 4 and 5, have qualitatively shown that the thalamus exhibited greater fluorescence than the hippocampus. The results of this paper also confirmed this quantitatively (see Fig. 7). This may be due to the distinct capillary density and/or the vascular architecture of the thalamus compared with the hippocampus [30]. The higher number of capillaries, or sites of potential BBB opening, may be the cause for increased permeation of agents. Another possible rationale for the difference in fluorescence may be due to the fact that the extracellular space varies in terms of structure and diffusion rate, which implies differences in the rate of diffusion of delivered agents once they exit the vascular system [44]. The exact reason remains unknown and these effects will be studied in more detail in the future.

Our experimental setup has several advantages, but the relatively small size of the mouse brain requires additional considerations, i.e., a 13.0-mm axial transducer focus was used, which was approximately 5 mm long in its ventral-dorsal axis. Therefore, the potential of standing waves needs to be considered. Standing-wave effects, as studied *in vitro* and in simulations under different acoustic conditions, include distortion of the beam shape and variation in the peak pressure [45]. However, our studies using the aforementioned acoustic parameters have indicated that these effects are not significant, i.e., the BBB opening region and location were in good agreement with the expected beam shape and location in both this (see Figs. 4 and 5) and previous studies [5], [10], [17], [46]. Also, different acoustic pressure amplitudes induced statistically significant differences in fluorescence intensity in this paper (see Fig. 6) and in previous studies using MRI [5]. We thus demonstrated clear pressure-dependent thresholds for BBB opening and it was, therefore, deemed highly unlikely that the observed changes in fluorescence were associated with standing wave effects. However, studies currently ongoing in our laboratory entail both simulations and *in vitro* skull experiments to verify the aforementioned assumptions [47].

The histological analysis in Figs. 8 and 9 depict 6-μm-thick, fluorescent unstained and H&E-stained slices that were sequentially sectioned. The H&E stained sections revealed that BBB opening, as indicated by the increased fluorescence, can occur without discrete damage sites. Therefore, there may be a workable threshold, in which no damage occurs. In fact, our preliminary analysis did not depict any histological damage (see Figs. 8 and 9). More in depth analysis and long-term histological studies need to be performed to determine the safety, stability, and persistence timeline of the size-isolated bubbles.

In conclusion, we have shown that in-house manufactured microbubbles, composed of DSPC- and PEG40S-lipid shells with a PFB-gas core, can be utilized for FUS-induced BBB opening. Differential centrifugation is a quick and robust means to size-isolate bubbles, and in this study, distinct size ranges of 1–2- and 4–5-μm in diameter were successfully generated. The BBB opening peak-rarefactional pressure threshold was significantly lower for 4–5-μm than for 1–2-μm bubbles. Assuming a constant microbubble concentration during systemic injection, a greater amount of dextran was trans-BBB delivered at any given pressure amplitude for the larger bubbles. Apart from size dependence, greater fluorescence in the thalamus compared with the hippocampus was observed, thus indicating regional variations. Preliminary histological evaluation indicated that our in-house manufactured, size-isolated bubbles do not induce histological damage at pressures near the threshold for BBB opening [48].

Acknowledgments

The authors would like to thank the Riverside Research Institute (New York, NY, USA) for providing the transducers used in this paper and J. Hui for the bubble characterization.

This work was supported by the National Science Foundation under Grant CAREER-0644713, the National Institutes of Health under Grant R21EY018505 and Grant R01EB009041, and by the Kinetics Foundation.

Biographies

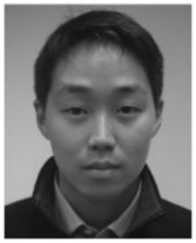

James J. Choi (S'06) received the B.S. degree in computer engineering from the University of Michigan, Ann Arbor, in 2004 and the M.S. degree in biomedical engineering from Columbia University, New York, NY, in 2006. He is currently working toward the Ph.D. degree in the Department of Biomedical Engineering, Columbia University.

He was engaged in undergraduate research with multielement arrays and nonlinear ultrasonic beam mixing. His current research interests include noninvasive and localized drug delivery and surgery.

Jameel A. Feshitan received the B.S. degree from the University of Missouri, Columbia, in 2007 and the M.S. degree from Columbia University, New York, NY, in 2008, both in chemical engineering. He is currently working toward the Doctoral degree with M. A. Borden in the Department of Chemical Engineering, Columbia University.

His current research interest includes development of multifunctional contrast agents.

Babak Baseri received the B.S. degree from Rutgers University, Piscataway, NJ, in 2005, and the M.S. degree from the University of Medicine and Dentistry of New Jersey, Newark, NJ, in 2008. He is currently working toward the medical degree with St. George's University, St. George, Grenada.

He was a full-time Research Scientist in the Department of Biomedical Engineering, Columbia University, New York, NY, from 2008 to 2009. His research interests include focused ultrasound-induced blood–brain barrier opening and neurodegenerative diseases.

Shougang Wang (M'07) received the B.S. degree from Tsinghua University, Beijing, China, in 1998 and the Ph.D. degree from Brown University, Providence, RI, in 2006.

He was a postdoctoral Research Scientist in the Department of Biomedical Engineering and the Department of Radiology, Columbia University, New York, NY, from 2006 to 2008. He is currently with the National Semiconductor Corporation, Santa Clara, CA, as an ultrasound Architect Engineer. His research interests include ultrasonic vibration potential imaging, conventional ultrasound imaging, cardiac elasticity imaging, and ultrasound aided drug delivery through the blood–brain barrier.

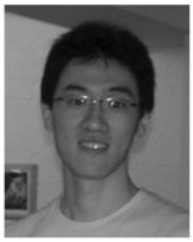

Yao-Sheng Tung was born in Taipei, Taiwan. He received the B.S. and M.S. degrees from National Taiwan University, Taipei. He is currently working toward the Ph.D. degree with the Department of Biomedical Engineering, Columbia University, New York, NY.

He was a Research Assistant with National Taiwan University Hospital, Taipei, in 2006. His current research interests include ultrasound therapy with microbubbles, and cavitation effects.

Mark A. Borden (M'04) received the Ph.D. degree in chemical engineering from the University of California (UC), Davis, in 2003.

He was with K. Ferrara in the Department of Biomedical Engineering, UC, from 2003–2007. Since 2007, he has been an Assistant Professor of chemical engineering, in the Department of Chemical Engineering, Columbia University, New York, NY. His current research interests include development of improved microbubble constructs for molecular imaging and targeted drug delivery.

Dr. Borden has received the New York State Office of Science, Technology and Academic Research James D. Watson Investigator Award.

Elisa E. Konofagou (M'06) received the B.S. degree in chemical physics from the Université de Pierre et Marie Curie, Paris VI, Paris, France, the M.S. degree in biomedical engineering from Imperial College of Physics, Engineering and Medicine, London, U.K., in 1992 and 1993, respectively. In 1999, she received the Ph.D. degree in biomedical engineering from the University of Houston, Houston, TX, for her work on elastography at the University of Texas Medical School, Houston. For her postdoctoral research, she focused on elasticity-based monitoring of focused ultrasound therapy from Brigham and Women's Hospital, Harvard Medical School, Boston, MA.

She is currently an Associate Professor of biomedical engineering and radiology, and Director of the Ultrasound and Elasticity Imaging Laboratory, Department of Biomedical Engineering and Department of Radiology, Columbia University, New York, NY. Her research interests include the development of novel elasticity imaging techniques and therapeutic ultrasound methods, myocardial elastography, electromechanical and pulse wave imaging, harmonic motion imaging, and focused ultrasound therapy and drug delivery in the brain, with several clinical collaborations in the Columbia Presbyterian Medical Center, New York, and elsewhere. She is the author of more than 110 published articles in the aforementioned fields.

Dr. Konofagou is a technical committee member of the Acoustical Society of America and the American Institute of Ultrasound in Medicine. She is also a technical committee member of the International Society of Therapeutic Ultra-sound, the Engineering in Medicine and Biology Conference, and the American Association of Physicists in Medicine. She is also an Associate Editor in the *Medical Physics Journal* and is the recipient of awards from the

American Heart Association, the Acoustical Society of America, the American Institute of Ultra-sound in Medicine, the Wallace H. Coulter foundation, the National Institutes of Health, the National Science Foundation, and the Radiological Society of North America.

References

[1]. Stewart PA, Tuor UI. Blood-eye barriers in the rat: Correlation of ultrastructure with function. J. Comp. Neurol. 1994; 340(4):566–576. [PubMed: 8006217]

[2]. Abbott NJ, Ronnback L, Hansson E. Astrocyte-endothelial interactions at the blood-brain barrier. Nat. Rev. Neurosci. 2006; 7(1):41–53. [PubMed: 16371949]

[3]. Pardridge WM. Drug targeting to the brain. Pharm. Res. 2007; 24(9):1733–1744. [PubMed: 17554607]

[4]. Hynynen K, McDannold N, Vykhodtseva N, Jolesz FA. Noninvasive MR imaging-guided focal opening of the blood-brain barrier in rabbits. Radiology. 2001; 220(3):640–646. [PubMed: 11526261]

[5]. Choi JJ, Pernot M, Brown TR, Small SA, Konofagou EE. Spatio-temporal analysis of molecular delivery through the blood-brain barrier using focused ultrasound. Phys. Med. Biol. 2007; 52(18):5509–5530. [PubMed: 17804879]

[6]. Sheikov N, McDannold N, Sharma S, Hynynen K. Effect of focused ultrasound applied with an ultrasound contrast agent on the tight junctional integrity of the brain microvascular endothelium. Ultrasound Med. Biol. 2008; 34(7):1093–1104. [PubMed: 18378064]

[7]. Hynynen K, McDannold N, Vykhodtseva N, Raymond S, Weissleder R, Jolesz FA, Sheikov N. Focal disruption of the blood-brain barrier due to 260-kHz ultrasound bursts: A method for molecular imaging and targeted drug delivery. J. Neurosurg. 2006; 105(3):445–454. [PubMed: 16961141]

[8]. Sheikov N, McDannold N, Jolesz F, Zhang YZ, Tam K, Hynynen K. Brain arterioles show more active vesicular transport of blood-borne tracer molecules than capillaries and venules after focused ultrasound-evoked opening of the blood-brain barrier. Ultrasound Med. Biol. 2006; 32(9):1399–1409. [PubMed: 16965980]

[9]. Sheikov N, McDannold N, Vykhodtseva N, Jolesz F, Hynynen K. Cellular mechanisms of the blood-brain barrier opening induced by ultrasound in presence of microbubbles. Ultrasound Med. Biol. 2004; 30(7):979–989. [PubMed: 15313330]

[10]. Choi JJ, Pernot M, Small SA, Konofagou EE. Noninvasive, transcranial and localized opening of the blood-brain barrier using focused ultrasound in mice. Ultrasound Med. Biol. 2007; 33(1):95–104. [PubMed: 17189051]

[11]. McDannold N, Vykhodtseva N, Hynynen K. Targeted disruption of the blood-brain barrier with focused ultrasound: Association with cavitation activity. Phys. Med. Biol. 2006; 51(4):793–807. [PubMed: 16467579]

[12]. McDannold N, Vykhodtseva N, Raymond S, Jolesz FA, Hynynen K. MRI-guided targeted blood-brain barrier disruption with focused ultrasound: Histological findings in rabbits. Ultrasound Med. Biol. 2005; 31(11):1527–1537. [PubMed: 16286030]

[13]. Kinoshita M, McDannold N, Jolesz FA, Hynynen K. Noninvasive localized delivery of Herceptin to the mouse brain by MRI-guided focused ultrasound-induced blood-brain barrier disruption. Proc. Nat. Acad. Sci. USA. 2006; 103(31):11719–11723. [PubMed: 16868082]

[14]. Raymond SB, Treat LH, Dewey JD, McDannold NJ, Hynynen K, Bacskai BJ. Ultrasound enhanced delivery of molecular imaging and therapeutic agents in Alzheimer's disease mouse models. PLoS ONE. 2008; 3(5):e2175. [PubMed: 18478109]

[15]. Treat LH, McDannold N, Vykhodtseva N, Zhang Y, Tam K, Hynynen K. Targeted delivery of doxorubicin to the rat brain at therapeutic levels using MRI-guided focused ultrasound. Int. J. Cancer. 2007; 121(4):901–907. [PubMed: 17437269]

[16]. Wang, S.; Choi, JJ.; Tung, Y-S.; Morrison, B., III; Konofagou, EE. Qualitative and quantitative analysis of the molecular delivery through the ultrasound-enhanced blood-brain barrier opening in the murine brain. presented at the IEEE Symp. Ultrason. Ferroelectr. Freq. Control; Beijing, China. 2008.

[17]. Choi JJ, Wang S, Tung Y-S, Morrison B III, Konofagou EE. Molecules of various pharmacologically-relevant sizes can cross the ultrasound-induced blood-brain barrier opening in vivo. Ultrasound Med. Biol. 2009 to be published.

[18]. Zlokovic BV. The blood-brain barrier in health and chronic neurode-generative disorders. Neuron. 2008; 57(2):178–201. [PubMed: 18215617]

[19]. Caskey CF, Kruse DE, Dayton PA, Kitano TK, Ferrara KW. Microbubble oscillation in tubes with diameters of 12, 25, and 195 microns. Appl. Phys. Lett. 2006; 88(3):033902-1–033902-3.

[20]. Caskey CF, Stieger SM, Qin S, Dayton PA, Ferrara KW. Direct observations of ultrasound microbubble contrast agent interaction with the microvessel wall. J. Acoust. Soc. Amer. 2007; 122(2):1191–1200. [PubMed: 17672665]

[21]. Stieger SM, Caskey CF, Adamson RH, Qin S, Curry FR, Wisner ER, Ferrara KW. Enhancement of vascular permeability with low-frequency contrast-enhanced ultrasound in the chorioallantoic membrane model. Radiology. 2007; 243(1):112–121. [PubMed: 17392250]

[22]. Zheng H, Dayton PA, Caskey C, Zhao S, Qin S, Ferrara KW. Ultrasound-driven microbubble oscillation and translation within small phantom vessels. Ultrasound Med. Biol. 2007; 33(12): 1978–1987. [PubMed: 17900793]

[23]. Qin S, Ferrara KW. The natural frequency of nonlinear oscillation of ultrasound contrast agents in microvessels. Ultrasound Med. Biol. 2007; 33(7):1140–1148. [PubMed: 17478030]

[24]. Sassaroli E, Hynynen K. Cavitation threshold of microbubbles in gel tunnels by focused ultrasound. Ultrasound Med. Biol. 2007; 33(10):1651–1660. [PubMed: 17590501]

[25]. Sassaroli E, Hynynen K. Resonance frequency of microbubbles in small blood vessels: A numerical study. Phys. Med. Biol. 2005; 50(22):5293–5305. [PubMed: 16264254]

[26]. Sassaroli E, Hynynen K. Forced linear oscillations of microbubbles in blood capillaries. J. Acoust. Soc. Amer. 2004; 115(6):3235–3243. [PubMed: 15237848]

[27]. Choi, JJ.; Wang, S.; Morrison, B., III; Konofagou, EE. Molecular delivery and microbubble dependence study of the FUS-induced blood-brain barrier opening in vivo. presented at the IEEE Symp. Ultrason. Ferroelect. Freq. Control; New York, NY. 2007.

[28]. Feshitan JA, Chen CC, Kwan JJ, Borden MA. Microbubble size isolation by differential centrifugation. J. Colloid Interface Sci. 2009; 329(2):316–324. [PubMed: 18950786]

[29]. Cavaglia M, Dombrowski SM, Drazba J, Vasanji A, Bokesch PM, Janigro D. Regional variation in brain capillary density and vascular response to ischemia. Brain Res. 2001; 910(1–2):81–93. [PubMed: 11489257]

[30]. Klein B, Kuschinsky W, Schrock H, Vetterlein F. Interdependency of local capillary density, blood flow, and metabolism in rat brains. Amer. J. Physiol. 1986; 251(6 Pt 2):H1333–H1340. [PubMed: 3098116]

[31]. Kvåle S, Jakobsen HA, Asbjørnsen OA, Omtveit T. Size fractionation of gas-filled microspheres by flotation. Separations Technol. 1996; 6(4):219–226.

[32]. Baseri B, Choi JJ, Tung YS, Konofagou EE. Safety assessment of blood-brain barrier opening using focused ultrasound and definity microbubbles: A short-term study. Ultrasound Med. Biol. in review.

[33]. Talu E, Hettiarachchi K, Zhao S, Powell RL, Lee AP, Longo ML, Dayton PA. Tailoring the size distribution of ultrasound contrast agents: Possible method for improving sensitivity in molecular imaging. Mol. Imag. 2007; 6(6):384–392.

[34]. Ganan-Calvo AM, Gordillo JM. Perfectly monodisperse microbubbling by capillary flow focusing. Phys. Rev. Lett. 2001; 87(27 Pt 1):274501-1–274501-4. [PubMed: 11800883]

[35]. Xu JH, Li SW, Wang YJ, Luo GS. Controllable gas-liquid phase flow patterns and monodisperse microbubbles in a microfluidic T-junction device. Appl. Phys. Lett. 2006; 88(13):133506-1–133506-3.

[36]. Farook U, Zhang HB, Edirisinghe MJ, Stride E, Saffari N. Preparation of microbubble suspensions by co-axial electrohydrodynamic atomization. Med. Eng. Phys. 2007; 29(7):749–754. [PubMed: 17035065]

[37]. Chomas JE, Dayton P, May D, Ferrara K. Threshold of fragmentation for ultrasonic contrast agents. J. Biomed. Opt. 2001; 6(2):141–150. [PubMed: 11375723]

[38]. Samuel S, Cooper MA, Bull JL, Fowlkes JB, Miller DL. An ex vivo study of the correlation between acoustic emission and microvascular damage. Ultrasound Med. Biol. 2009; 35(9):1574–1586. [PubMed: 19560856]

[39]. Chen S, Shohet RV, Bekeredjian R, Frenkel P, Grayburn PA. Optimization of ultrasound parameters for cardiac gene delivery of adenoviral or plasmid deoxyribonucleic acid by ultrasound-targeted microbubble destruction. J. Amer. Coll. Cardiol. 2003; 42(2):301–308. [PubMed: 12875768]

[40]. Rockenstein E, Crews L, Masliah E. Transgenic animal models of neurodegenerative diseases and their application to treatment development. Adv. Drug Del. Rev. 2007; 59(11):1093–1102.

[41]. Coyle P. Spatial features of the rat hippocampal vascular system. Exp. Neurol. 1978; 58(3):549–561. [PubMed: 620709]

[42]. Coyle P. Arterial patterns of the rat rhinencephalon and related structures. Exp. Neurol. 1975; 49(3):671–690. [PubMed: 1204702]

[43]. Coyle P. Vascular patterns of the rat hippocampal formation. Exp. Neurol. 1976; 52(3):447–458. [PubMed: 954917]

[44]. Sykova E, Nicholson C. Diffusion in brain extracellular space. Physiol. Rev. 2008; 88(4):1277–1340. [PubMed: 18923183]

[45]. Baron C, Aubry JF, Tanter M, Meairs S, Fink M. Simulation of intracranial acoustic fields in clinical trials of sonothrombolysis. Ultra-sound Med. Biol. 2009; 35(7):1148–1158.

[46]. Choi JJ, Wang S, Brown TR, Small SA, Duff KE, Konofagou EE. Noninvasive and transient blood-brain barrier opening in the hippocampus of Alzheimer's double transgenic mice using focused ultrasound. Ultrason. Imag. 2008; 30(3):189–200.

[47]. Deffieux, T.; Konofagou, EE. AIUM Annual Convention. San Diego, CA: 2010. Transcranial focused ultrasound for blood-brain barrier opening—Numerical simulations with *in vitro* validation in human and monkey skulls. abstract for the

[48]. Konofagou, EE.; Choi, JJ.; Baseri, B.; Tung, Y-S. Mechanism and safety at the threshold of blood-brain barrier opening. presented at the Int. Symp. Therapeutic Ultrasound, Aix En Provence; France. 2009.

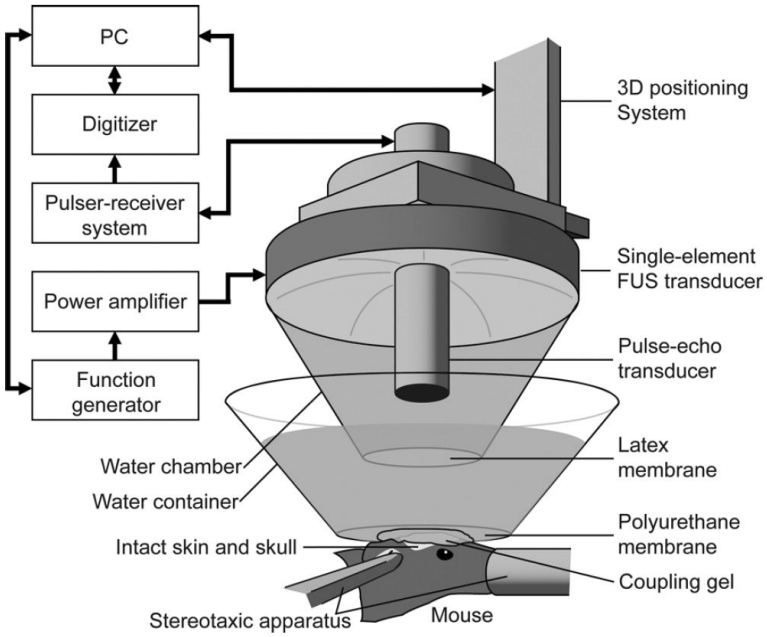

Fig. 1.
In vivo FUS-induced BBB opening experimental setup.

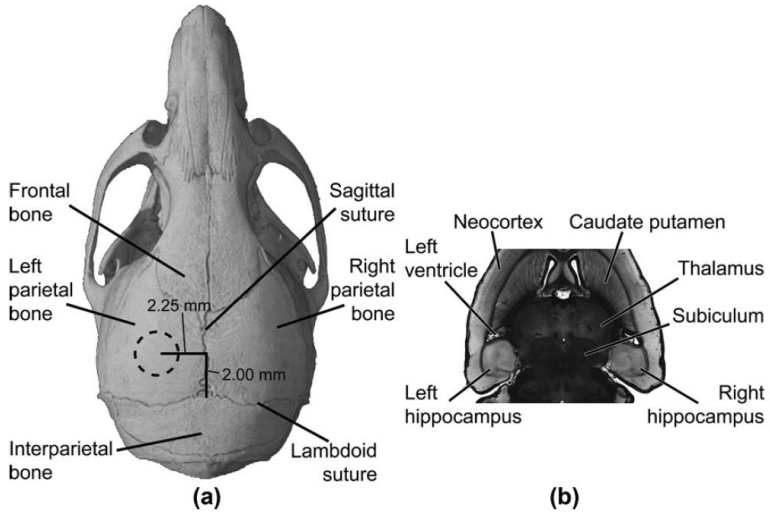

Fig. 2.

Acoustic waves propagated through (a) left parietal bone and converged to a 1.32-mm diameter region (dotted circle). (b) Left hippocampus was targeted while the right region acted as a control.

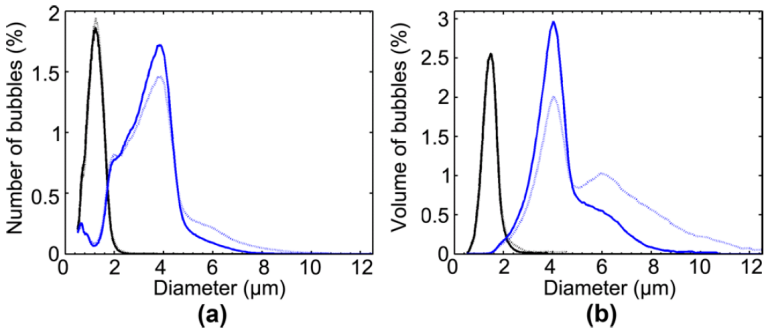

Fig. 3.

Size distributions of microbubbles are depicted as (a) number-weighted percent of the total concentration of bubbles and (b) volume-weighted percent of the total volume of bubbles. Distinct peaks at approximately 1–2 μm (solid black) and 4–5 μm (solid blue) are visible. After sonication, the microbubbles were reanalyzed (dashed), depicting little deviation of its mean or median diameters.

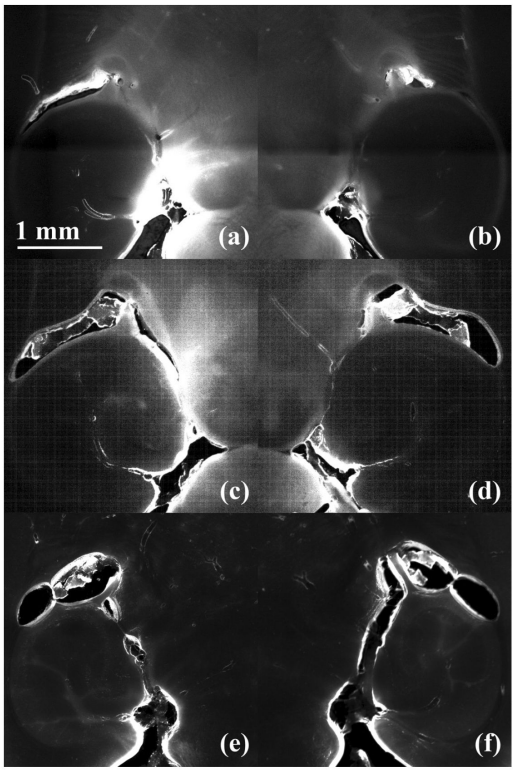

Fig. 4.

Fluorescence images of the (a, c, and e) left and (b, d, and f) right brain regions. Delivery of 3 kDa dextran by sonication of the left region in the presence of 1–2 μm bubbles resulted in a fluorescence increase at (a) 0.61 and (c) 0.46 MPa, but not (e) 0.30 MPa.

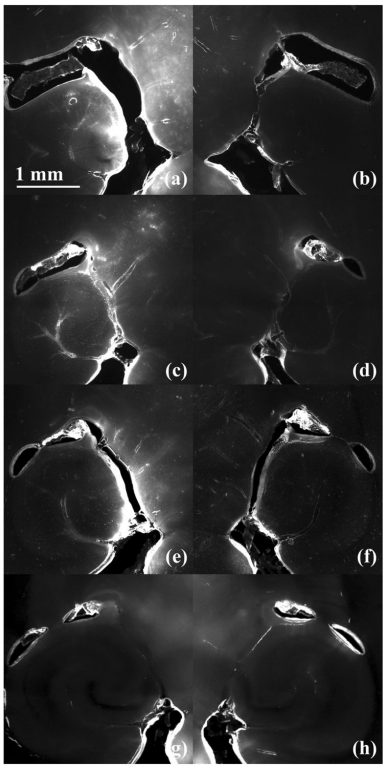

Fig. 5.

Fluorescence images of the (a, c, e, and g) left and (b, d, f, and h) right brain regions. Delivery of 3 kDa dextran by sonication of the left region in the presence of 4–5 μm bubbles resulted in a fluorescence increase at (a) 0.61 (c) 0.46, and (e) 0.30 MPa, but not (g) 0.15 MPa.

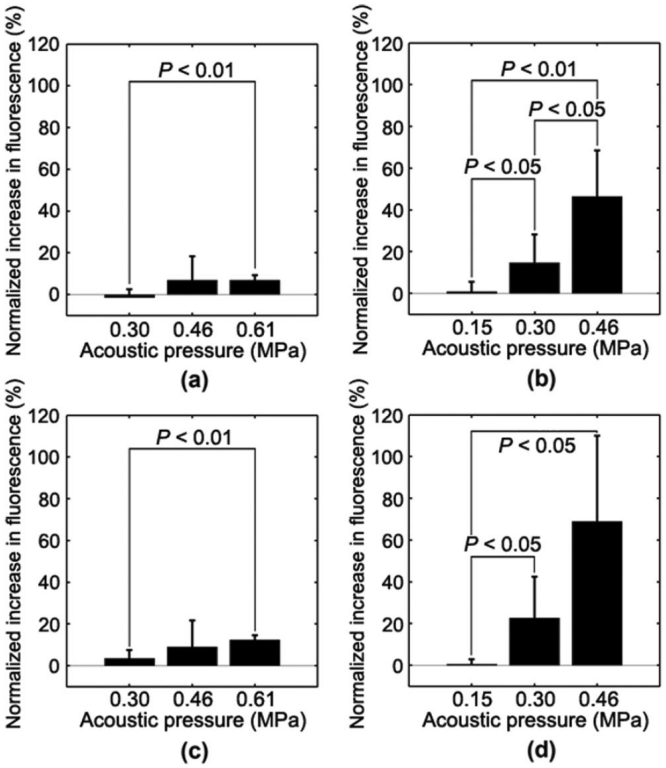

Fig. 6.

Fluorescence increase of the left (a, b) hippocampi and (c, d) thalami relative to the right corresponding region at different acoustic pressures and microbubbles. With (a, c) 1–2 μm bubbles, no significant BBB opening was observed at 0.30 or 0.46 MPa while opening was observed at 0.61 MPa in both regions. With (b, d) 4–5 μm bubbles, no significant BBB opening was observed at 0.15 MPa while opening was observed at 0.30 and 0.46 MPa in both regions. A significant increase in fluorescence was also observed in the hippocampus at 0.46 MPa over 0.30 MPa.

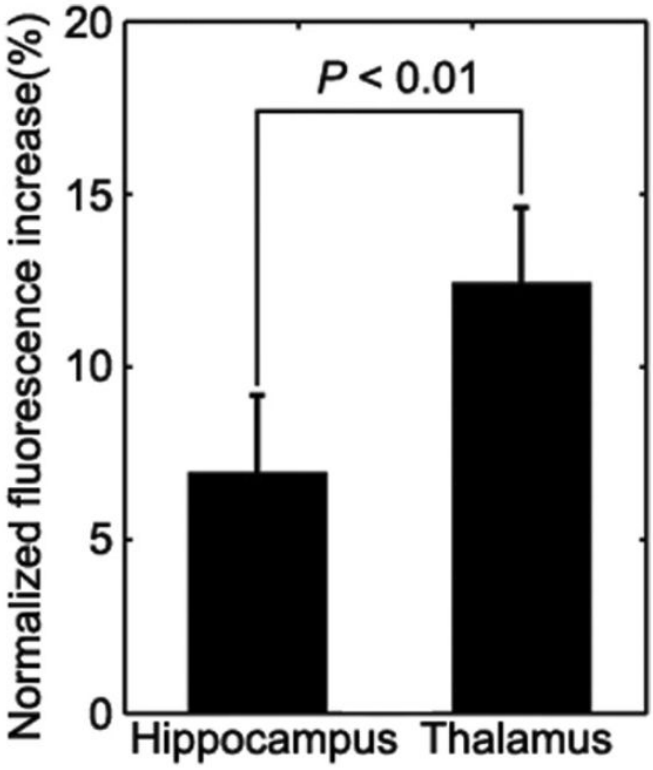

Fig. 7.

Increase in average fluorescence of the left ROI relative to the right ROI due to sonication at 0.61 MPa after the intravenous injection of 1–2 μm bubbles. A significantly greater fluorescence was observed in the thalamus when compared with the hippocampus.

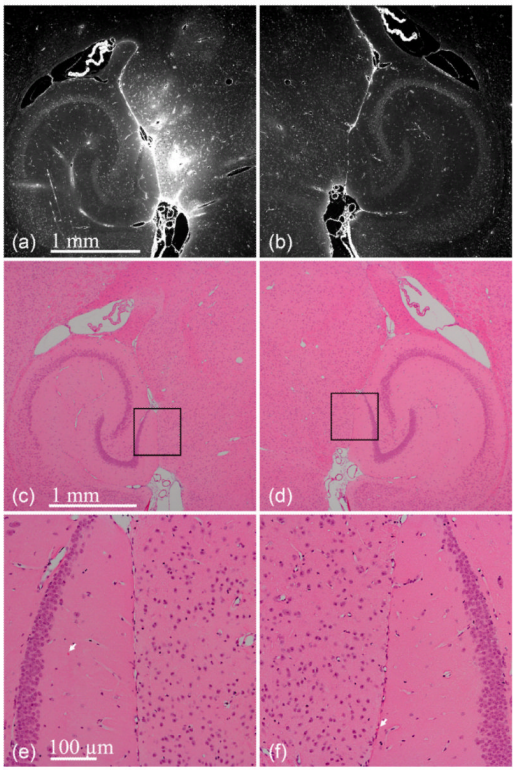

Fig. 8.

Paraffin-embedded 6-μm thick brain sections after sonicating the (a, c, and e) left ROI at 0.46 MPa in the presence of 1–2 μm bubbles. The (b, d, and f) right was the control. Increased fluorescence in the (a) left ROI indicates delivery of 3 kDa dextran. Hematoxylin and eosin sections reveal no macroscopic damage. White arrows indicate erythrocytes, but may be artifacts due to histological techniques since they were observed on both hemispheres. The black boxes in (c) and (d) refer to the ROIs of (e) and (f).

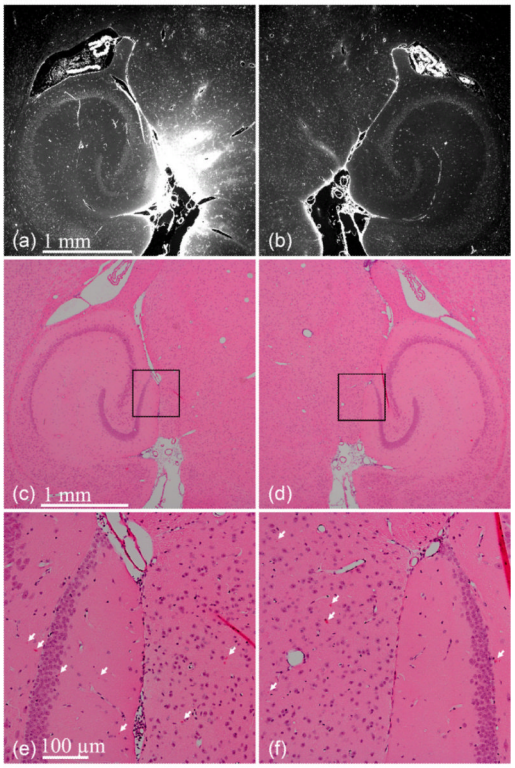

Fig. 9.

Paraffin-embedded 6-μm thick brain sections after sonicating the (a, c, and e) left ROI at 0.3 MPa in the presence of 4–5 μm bubbles. (b, d, and f) Right ROI was the control. Increased fluorescence in the (a) left ROI indicates delivery of 3 kDa dextran. Hematoxylin and eosin sections reveal no macroscopic damage. White arrows indicate erythrocytes, but may be artifacts due to histological techniques since they were observed on both hemispheres. The black boxes in (c) and (d) refer to the ROIs of (e) and (f).

TABLE I

Summary of Microbubble Size Distribution

	Number-weighted diameter (μm)		Volume-weighted diameter (μm)		
	mean ±std.	**median ±std.**	**mean ±std.**	**median ±std.**	**PI**
1–2 μm bubbles					
Pre-experiment	1.2±0.1	1.2±0.1	1.5±0.2	1.5±0.1	1.3±0.1
Post-experiment	1.4±0.2	1.3±0.1	2.9±1.5	2.6±1.5	2.1±0.9
4–5 μm bubbles					
Pre-experiment	3.3±0.1	3.4±0.1	5.0±0.2	4.3±0.1	1.5±0.1
Post-experiment	3.2±0.2	3.2±0.2	4.6±0.4	4.3±0.2	1.4±0.1